PROCEEDINGS, 41st Workshop on Geothermal Reservoir Engineering
Stanford University, Stanford, California, February 22-24, 2016
SGP-TR-209

Analysis of Natural Fracture Shear Slip and Propagation in Response to Injection

Amirhossein Kamali, Ahmad Ghassemi

Mewbourne School of petroleum & Geological Engineering, The University of Oklahoma, Norman, OK 73019

ahmad.ghassemi@ou.edu

a.kamali@ou.edu

Keywords: Natural fracture Propagation, Closed Crack, Mixed-Mode Propagation, Nonlinear Joint, Displacement Discontinuity

ABSTRACT

Geothermal reservoir stimulation by shear slip on pre-existing fractures has been proposed as the main permeability enhancement mechanism. In recent years, this has been interpreted by some to exclude the possibility of natural fracture propagation in tensile mode. However, fracture mechanics studies have shown that propagation of mechanically-closed cracks under compressive stresses often involves both mode I and mode II propagation. The former is known as a wing crack, an out-of-plane growth of the pre-existing closed cracks triggered by the shear deformation of crack surfaces. Once initiated, the wing cracks tend to deviate and extend in the direction of the maximum compressive stress. However, crack extension along the initial shear surface also occurs. The relative dominance of each of these propagation modes is a function of the in-situ stress state, and pore pressure, and rock properties. A displacement discontinuity method with Mohr-Coulomb elements is used in this paper to study the response of natural fractures to injection. Modeling results indicate that the onset of fracture slip occurs when the initial shear stress exceeds the shear strength of the Mohr-Coulomb contact elements. Wing cracks form and propagate with an angle from the pre-existing crack and turn toward the maximum compressive stress afterward. "Shear" cracks may start to form, along with the tensile wing cracks, in a plane approximately parallel to the pre-existing natural fracture. These types of propagation can lead to coalescence of multiple fractures and formation of a fracture network.

1. INTRODUCTION

EGS design concept in a number of field projects (Soultz, Desert Peak, Newberry) relied on the conceptual model of permeability increase by induced slip on natural fractures due water injection. The conceptual model envisions injection pressures below the minimum in-situ stress to cause slip on the critically-stressed fractures and or induce shear failure of the rock mass. However, Jung (2013) presented a review of the results and observations from a number of EGS experiments and suggested that the adherence to stimulation by shear or "hydro-shearing" is the main reason for the poor progress in the EGS success. Based on interesting interpretations of a number of phenomena, Jung argued that tensile fracturing and not shear slip or propagation is the main mechanism of stimulation, recommending a return to the conventional stimulation concept. In this paper, we review the concept of wing-crack propagation and show this mechanism is in fact, an integral part of the shear slip stimulation mechanism and that a shear propagation mode is also plausible and can contribute to permeability and MEQ. The process is similar to the shear failure in laboratory triaxial compression tests on rock whereby tensile and shear cracks coalesce to form a macroscopic shear crack or fault across the sample. And although individual tensile cracks do form in the process, the failure is referred to as shear failure.

Propagation of closed fractures has been investigated under uniaxial and biaxial compressive stresses. Extensive research has been done on the propagation of wing cracks including the early works of Bombolakis (1973), Hoek and Bieniawksi (1984), Horii and Nemat-Nasser (1986). Both of Bombolakis (1973), Nemat-Nasser and Horri (1983), and Horri and Nemat-Nasser (1986) conducted experiments on open flaws in C.R.39 photoloelastic plates. Hoek and Bieniawski (1984) studied the failure of open cracks in glass samples under compression. Formation and extension of wing cracks in dry closed cracks has been studied analytically, numerically and by means of experiment under different loading conditions (Shen and Stephansson1994; Bobet and Eisntein, 1998) in the general context of rock failure.

In this study we analyze fracture slip and propagation in response to injection and investigate the conditions which favor each of mode I and Mode II propagation in a hydro-mechanically coupled system. Modelling results can be used in geothermal systems to predict the connectivity patterns among natural fractures and plausible mechanisms in different zones of the reservoir.

2. MODEL DEVELOPMENT

While wing crack propagation, which is essentially Mode I opening caused by shear on the main crack, has been investigated for the past few decades, Mode II propagation and the co-existence of mode I and II has not been considered despite the fact that it has been observed experimentally. As Rao et al. (2003) have discussed, under compression-shear loading conditions, mode I stress intensity factor often reaches its maximum before the mode II stress intensity factor and since Mode I toughness K_{IC} is generally lower than that of mode II, K_{IIC}, cracks propagate in mode I (wing crack) first. However, it is important to note that the shear stress concentration in the vicinity of the kink point may exceed the shear strength of the material due to further shearing on the crack surfaces which gives rise to Mode II crack propagation. In fact, experimental (Petit and Barquins 1988) and numerical results (Shen and Stephansson 1994; Bobet and Einstein 1998) indicate that Mode II propagation is present along with mode I propagation in closed cracks under compression-shear loading condition.

However, the analysis of closed cracks is challenging as there are no widely accepted failure criteria for such cracks. This motivated Huang et al. 2013 to use the VMIB for modeling the propagation of natural fractures. Furthermore, the presence of friction and dilatancy adds to the complexity of closed crack analysis (Scavia 1995). The initial crack remains mechanically closed under compression while the wing cracks are open throughout the loading. Formation of secondary cracks that are in-plane with the pre-existing cracks has been reported in several works (Shen and Stephansson 1994; Bobet and Einstein 1998; Vesarhelyi and Bobet 2000; Li et al. 2005; Cao et al. 2015). These in-plane secondary cracks form at the tip of the flaws as shear fractures. Additional difficulties are associated with modelling the latter case as the contact properties of the newly formed elements (i.e. contact elements) are usually not known (Dobroskok et al. 2005).

In this work we develop and use a displacement discontinuity (DD) model to simulate slip along a natural fracture and to examine the extension of wing and shear cracks. Pre-existing cracks can be approximated with M elements (boundary elements) and the elemental state of stress is prescribed at each step of loading. The induced shear and normal stress at a boundary element i is calculated using (Crouch and Starfield, 1979):

$$\overset{i}{\sigma}_s = \sum_{j=1}^{M} \overset{ij}{A}_{ss} \overset{j}{D}_s + \sum_{j=1}^{M} \overset{ij}{A}_{sn} \overset{j}{D}_n \tag{1}$$

$$\overset{i}{\sigma}_n = \sum_{j=1}^{M} \overset{ij}{A}_{ns} \overset{j}{D}_s + \sum_{j=1}^{M} \overset{ij}{A}_{nn} \overset{j}{D}_n \tag{2}$$

where $\overset{i}{\sigma}_s$ and $\overset{i}{\sigma}_n$ are the shear and normal stresses at element i, D_s and D_n are the shear and normal displacement discontinuities along element i, and $\overset{ij}{A}_{pq}$ ($p,q=s,n$) are the influence coefficients. The unknown DD values are calculated by solving the $2M$ linear equations simultaneously using conventional methods of solving system of linear equations. It should be noticed that the total number of elements, M, is not constant and may increase as a result of propagation at the tip of the crack. Therefore, it is important to account for the increasing number of elements which is reflected in the size of influence coefficients and boundary condition matrices.

2.1 Contact Elements

Natural fracture deformation in the normal (transverse) direction is linked to the normal (shear) stress of the contact element through normal (shear) stiffness as follows,

$$\Delta \overset{i}{\sigma}_n = K_n \Delta \overset{i}{D}_n \tag{3}$$

$$\Delta \overset{i}{\sigma}_s = K_s \Delta \overset{i}{D}_s \tag{4}$$

where K_n and K_s are the normal and shear stiffness, respectively. It should be noted that **Eq. 4** holds only when the contact element is in the 'stick' condition. In other words, **Eq. 4** cannot be used when the contact element yields in the transverse direction.

A constant stiffness model can be simply implemented in a closed crack model to quantify the natural fracture deformation in the normal and transverse direction. However, a nonlinear joint deformation model might be a more realistic choice as most cracks exhibit a nonlinear closure behavior to some extent (Bandis et al. 1983; Brown and Scholz 1985; Cook 1992; Goodman 1976; Kamali and Pournik 2015). A Barton-Bandis model is used in this study to capture the nonlinearity in the closure behavior of the closed crack. The normal stress and the normal displacement discontinuity are related as follows:

$$\sigma_n = \frac{K_{ni} D_n}{1 - D_n / D_{\max}} \tag{5}$$

where K_{ni} is the initial normal stiffness and D_{max} is the maximum closure allowed between the fracture surfaces. It should be noted that closure is treated positive while opening is treated negative in this study. The contact element remains mechanically closed as long as the total normal stress acting on the element remains positive. The implementation of a non-linear stiffness model such as Barton-Bandis model is relatively simple in case of fracture closure simulation. However, the fracture opening simulation is found to be more difficult to handle as compared to closure simulation. The central difference formulation overestimates the stiffness and underestimates the total normal stress which becomes problematic when dealing with the opening of closed elements.

The shear stiffness, on the other hand, is assumed to be constant and the shear deformation is calculated based on **Eq. 4** before the element yields. After failure, its shear stiffness may instantaneously go to zero or some finite value depending on the type friction law used in the model.

2.2 DD Equations for Contact Elements

The DD equations can be re-arranged for the contact elements by considering the shear and normal stiffness and the effect of farfield stresses and be written as follows,

$$\overset{i}{\sigma_s^{\infty}} + \sum_{j=1}^{M} (\overset{ij}{A_{ss}} - \delta_{ij} K_s) \overset{j}{D_s} + \sum_{j=1}^{M} \overset{ij}{A_{sn}} \overset{j}{D_n} = 0 \tag{6}$$

$$\overset{i}{\sigma_n^{\infty}} + \sum_{j=1}^{M} \overset{ij}{A_{ns}} \overset{j}{D_s} + \sum_{j=1}^{M} (\overset{ij}{A_{nn}} - \delta_{ij} K_n) \overset{j}{D_n} = 0 \tag{7}$$

where δ_{ij} is the Kronecker's delta function,

$$\delta_{ij} = \begin{cases} 1 & i = j \\ 0 & i \neq j \end{cases} \tag{8}$$

It should be noted that **Eq. 6** and **7** are only applicable to the elements that are in the stick condition. It is important to keep track of the total stress on each element in order to determine the state of contact. DD elements are in 'stick' condition if the following condition is met,

$$|\, \overset{i}{(\sigma_s)_{tot}^{k}} \,| < c + |\, \overset{i}{(\sigma_n)_{tot}^{k}} \,| \tan\phi \tag{9}$$

where $\overset{i}{(\sigma_s)_{tot}^{k}}$ is the total shear stress along element *i* at the k^{th} step of loading, *C* is the natural fracture cohesion and ϕ is the friction angle. The elemental state of contact changes from 'stick' to 'slip' if the calculated shear stress exceeds the shear strength at a given normal stress. For a DD element in the 'slip' condition, the shear stress boundary condition should be adjusted such that it meets the Mohr-Coulomb criterion (see also Ghassemi et al., 2007):

$$\mathrm{sgn}(\tau_f^k)\, |\, \tau_f^k \,| - \overset{i}{(\sigma_s)_{tot}^{k-1}} = \sum_{j=1}^{M} \overset{ij}{A_{ss}}\, \Delta \overset{i}{D_s} + \sum_{j=1}^{M} \overset{ij}{A_{sn}}\, \Delta \overset{i}{D_n} \tag{10}$$

where τ_f^k is the shear strength determined from the Mohr-Coulomb criterion. Notice that **Eq. 10** should be used instead of **Eq. 6** when a DD element is in the slip condition. A Mohr-Coulomb element may change from stick to slip state from one stage of loading to another and also from one iteration to another within a particular loading step. Changing element's status from 'stick' to 'slip' within a particular stage of loading may reduce the rate of convergence and at some cases fails to converge. The reason for such behavior is that changing element's status affects the stress distribution on the neighboring elements which may cause oscillation in the iterative procedure.

2.3 Hydro-Mechanical Coupling

A hydro-mechanical coupling scheme is outlined in this section. The changes in displacement discontinuity are believed to be affected by the fluid pressure and vice versa. Therefore, a two-way coupling method is utilized here to capture the interaction between the fluid flow and fracture deformation.

The fluid flow problem is solved by discretizing the following continuity equation for the case of single phase, incompressible fluid,

$$\frac{\partial q}{\partial x}+\frac{\partial w}{\partial t}=0 \tag{11}$$

where q is the volumetric flow rate per unit thickness and w is the fracture aperture. It should be noticed that the flow rate used here is the volumetric flow rate per unit thickness of the DD elements. The flow rate can be expressed in terms of pressure gradient based on the lubrication theory,

$$\frac{\partial}{\partial x}\left(\frac{-k(wh')}{\mu h'}\frac{\partial p}{\partial x}\right)+\frac{\partial w}{\partial t}=0 \tag{12}$$

where h' is the thickness of the DD element, μ is the fluid viscosity, and k is fracture permeability. Permeability can be expressed in terms of aperture using cubic law and the changes in aperture, w, can also be expressed in terms of changes in normal DD,

$$\frac{\partial}{\partial x}\left(\frac{w^3}{12\mu}\frac{\partial p}{\partial x}\right)+\frac{\partial D_n}{\partial t}=0 \tag{13}$$

One can write the aperture in terms of aperture from the previous time step which are known and the changes in the normal displacement discontinuity as follow,

$$w_i^k = w_i^{k-1} - \Delta \overset{i}{D}_n \tag{14}$$

An implicit finite difference scheme with variable grid sizes is used along with the DD equations to solve the fluid flow and coupling components. It should be noticed that since the fracture aperture at the current time step is unknown, an iterative scheme is required to update the aperture values within a certain time step until error tolerance is reached. The final set of equations to be solved for a hydro-mechanically coupled system is as follows,

$$\begin{cases} \sum_{j=1}^{M} \overset{ij}{A}_{ss}\,\Delta \overset{j}{D}_s + \sum_{j=1}^{M} \overset{ij}{A}_{sn}\,\Delta \overset{j}{D}_n - K_s\,\Delta \overset{i}{D}_s = 0 \\ \sum_{j=1}^{M} \overset{ij}{A}_{ns}\,\Delta \overset{j}{D}_s + \sum_{j=1}^{M} \overset{ij}{A}_{nn}\,\Delta \overset{j}{D}_n - K_n\,\Delta \overset{i}{D}_n - (p_i^k - p_i^{k-1}) = 0 \\ T_{i-1/2}^k\, p_{i-1}^k - (T_{i-1/2} + T_{i+1/2})^k\, p_i^k + T_{i+1/2}^k\, p_{i+1}^k + \dfrac{\Delta \overset{i}{D}_n}{\Delta t} + \dfrac{\overset{i}{q}_{inj}}{L} = 0 \end{cases} \tag{15}$$

where q is the injection rate per unit thickness ,L is the length of the source element, and T_i are the transmissibility terms written as,

$$T_{i-1/2}^k = \frac{1}{8\times 12\times \mu}\left(\frac{2}{\Delta x_i(\Delta x_i + \Delta x_{i-1})}\right)(w^k{}_i + w^k{}_{i-1})^3 \tag{16}$$

Δx_i represents the ith element grid size.

2.4 Closed Crack Propagation Scheme

Several crack propagation criteria have been proposed over the years and they generally fall into these categories: the maximum tensile stress criterion, the minimum strain energy density criterion (S-criterion), and the maximum energy release rate criterion (G-criterion). Shen and Stephansson (1994) state that the direction of secondary shear propagation predicted by the S-criterion are not aligned with the correct direction of shear propagation. Shen and Stephansson (1994) also mention that the G-criterion works for a crack subject to tension and fails to work for cracks under compression. Therefore, they use a modified G-criterion to capture Mode I/II crack

propagation. The original G-criterion and the modified G-criterion are computationally intensive and may lose their advantage for fully coupled systems. Dobroskok et al. (2005) propose a unified crack propagation scheme in whih the mode and direction of crack propagation can be effectively found under mixed-mode loading conditions. Although, the proposed criterion by Dobroskok et al. (2005) allows for switching between mode I and mode II propagations, the scheme does not address the coexistence of wing crack and secondary shear cracks. Bobet and Einstein (1998) use a stress analysis approach to find the direction and mode of crack propagation.

While crack surfaces are separated and open in the case of hydraulic fracturing and the process is essentially a tensile-dominated propagation, the pre-existing fractures remain closed or partially closed throughout the propagation. Wing crack propagation occurs in mode I or opening mode, but it is caused by shear slip along the pre-existing crack surfaces. The equivalent stress intensity factor is used in this study to capture the growth of wing cracks:

$$K_{eq} = \frac{1}{2}\cos(\frac{\theta}{2})[K_I(1+\cos(\theta) - 3K_{II}\sin(\theta)] \tag{17}$$

where θ is the angle measured counter-clockwise from the tip of the crack, K_I and K_{II} are the mode I and II stress intensity factors, respectively which are determined directly from the normal and shear DD values as follows:

$$K_I = -\frac{E}{8(1-\nu^2)}\sqrt{\frac{2\pi}{a}}D_n \tag{18}$$

$$K_{II} = -\frac{E}{8(1-\nu^2)}\sqrt{\frac{2\pi}{a}}D_s \tag{19}$$

where E is the Young's modulus of the surrounding rock, ν is the Poisson's ratio, a is the half-length of the tip element and D_n and D_s are the normal and shear displacement discontinuity at the tip element. The wing cracks start to propagate once the equivalent stress intensity factor, K_{eq}, reaches the mode I fracture toughness, K_{IC}, and the angle of propagation is determined from the following equation (Stone and Babuska, 1997):

$$\theta = \begin{cases} 0 \\ 2\arctan\left(\frac{1}{4}(\frac{K_I}{K_{II}} - \mathrm{sgn}(K_{II})\sqrt{8+(\frac{K_I}{K_{II}})^2}\right) \end{cases} \tag{20}$$

Stress analysis is carried out at each time step before and after the wing crack propagation to find the local stresses (shear/normal) in the vicinity of the kink points. Local shear stresses are then compared to the shear strength obtained from the Mohr-Coulomb criterion. Shear propagation occurs once the local shear stress exceeds the shear strength at that point:

$$\sigma_s(\theta) > c' + \sigma_n(\theta)\tan\phi' \tag{21}$$

Notice that c' and ϕ' are the cohesion and friction angle of the intact rock and differs from the natural fracture frictional parameters c and ϕ. It is worth mentioning that the shear strength varies on different planes (different θ) ahead of the kink point and therefore, assigning a single critical shear strength may not serve as the proper shear propagation criterion.

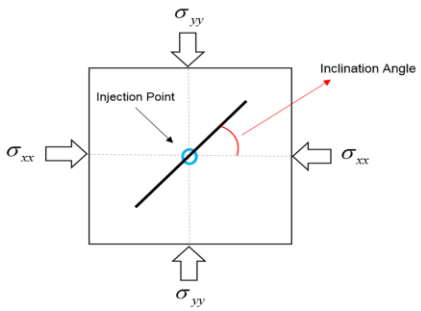

Figure 1. Schematic of crack geometry and in-situ stresses.

3. RESULTS

The following examples are designed to demonstrate the natural fracture propagation due to injection under various conditions. The impact of crack inclination angle, in-situ stress state, and rock frictional parameters on the propagation of mechanically-closed natural fractures is investigated in this section. Figure 1 shows a general schematic of the problem geometry. Notice that the crack inclination angle is measured counter-clockwise from the x-axis. Water is injected in the center of the closed natural fracture that causes normal and shear displacements. Water injection reduces the effective normal stress on the natural fracture, thus reducing the natural fracture closure (increases opening). It should be noted that the natural fracture may remain mechanically closed while its hydraulic aperture increases. Further injection may cause slip on the natural fracture which, in turn, results in wing crack initiation. Shear propagation (mode II) also occurs once the shear stress at the kink point exceeds intact rock shear strength.

3.1 Crack Inclination Angle

Three cracks with different angles from the x-axis are studied in this example. The initial natural fracture length is 2.8 m and it is similar in all cases. Cracks are subject to a tress field of 30 MPa in the *x*-direction and 50 MPa in the *y*-direction. Other parameters used in this example are summarized in Table 1. It can be observed in Figure 2 that the crack geometry looks similar for different inclination angles in the sense that the propagation is dominated by the formation of a wing crack. However, the pressure profile in Figure 3 shows that the 45 and 60 degree cracks require less pressure for propagation and growth as compared to the 30 degree crack. It is interesting to notice that for all crack angles, the pressure inside the crack is less than the minimum principal stress (σ_{xx}). It should also be noticed that the pre-existing crack remains mechanically closed or at least partially closed as wing cracks propagate. This example shows that the pressure requirement for wing crack propagation is lower at higher dip angles although the propagation trajectory is not significantly different between these cases. Moreover, the tendency for shear propagation is found to be higher at larger inclination angles as can be observed in Figure 2. Although the extension of the shear crack at the kink point is not significant in this example but it shows that mode II propagation may also occur.

Table 1. Parameters used in the crack angle analysis

Property	Value	Property	Value
σ_{yy} (MPa)	50	Natural fracture Friction Angle (deg)	15
σ_{xx} (MPa)	30	Natural fracture Cohesion (MPa)	0.50
Young's Modulus (GPa)	50	Maximum Closure (mm)	0.30
Poison's Ratio	0.25	Initial Hydraulic Aperture (mm)	0.10
Normal Stiffness (GPa)	500	K_{IC} (MPa.m$^{1/2}$)	2.0
Shear Stiffness (GPa)	5000	Fluid Viscosity (Pa.S)	1.0 e-3
Intact Rock Cohesion (MPa)	10	Injection Rate/unit thickness (m^2/s)	4.0 e-6
Intact Rock Friction Angle (deg)	25	Inclination Angle (deg)	30, 45, 60

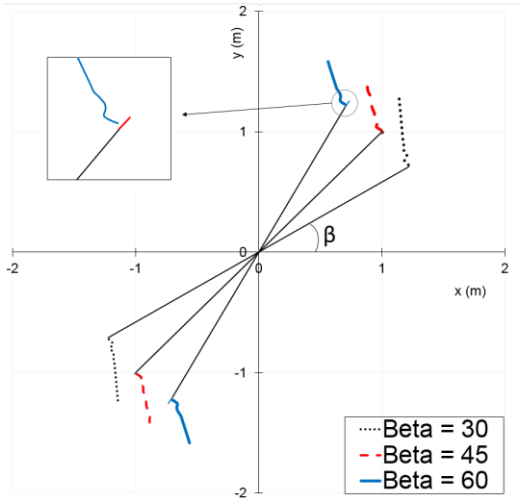

Figure 2. Wing crack propagation in three different crack angles.

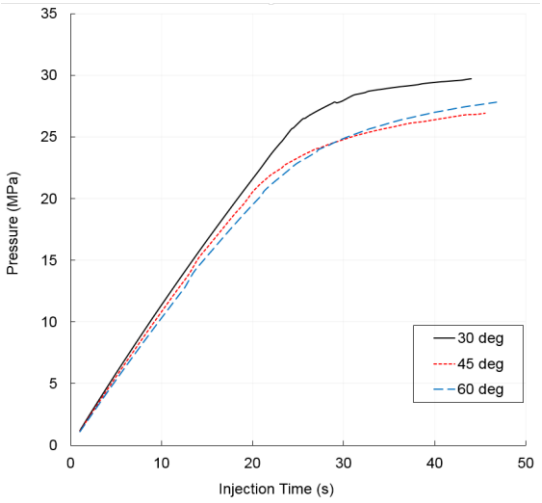

Figure 3. Pressure-Time profile at the injection point on the natural fracture.

3.2 Stress State, Constant Confining Stress

The following example is designed to study the impact of differential stress (i.e., $\sigma_{yy} - \sigma_{xx}$) at a constant confining stress. In this example a 45 degree crack with the initial length of 2.8 m is under 35 MPa of confining stress, namely, σ_{xx}, and the major principal stress takes values of 40, 50, and 60 MPa. Intact rock cohesion is set to 15 MPa and the rest of the parameters used in this example are listed in Table 1. Figure 4 shows the crack geometry for this example. It can be seen that the wing cracks look similar in these examples. The total shear deformation observed at the injection point is presented in Figure 5. It can be observed that the total shear slip starts to increase once the effective normal stress is reduced to a critical value due to injection. Additionally, the amount of total shear displacement is higher when the differential stress is higher. It is worth noticing the difference in the pressure-time profile at the injection point for these cases. It can be seen in Figure 6 that the pressure increases to almost as high as the minimum principal stress before the propagation begins for the case of the lowest differential stress. The pressure remains constant as the crack propagates. On the other hand, natural fracture propagation begins at pressures lower than the minimum in-situ stress for the cases with higher initial differential stress. As a result higher differential stress and confining pressure seems to favor propagation of shear cracks. It should be noticed when the propagation starts at pressures lower than the minimum principal stress, the pressure at the tip of wing cracks may not be sufficient to maintain the propagation and therefore the pressure must be increased (see Figure 6 for $\sigma_{yy} = 50$ and $\sigma_{yy} = 60$ MPa).

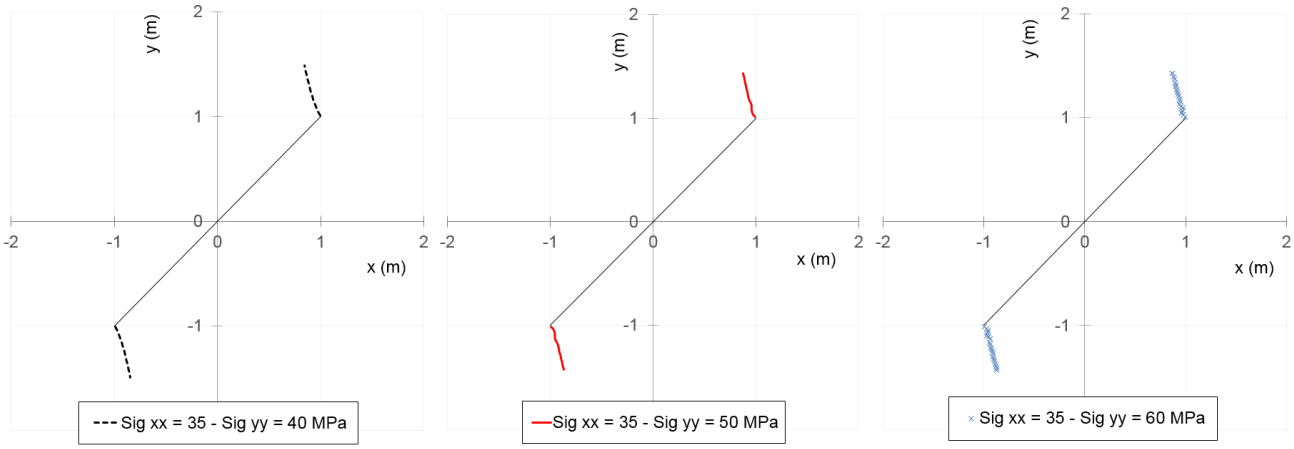

Figure 4. Crack trajectory for the constant confining stress example.

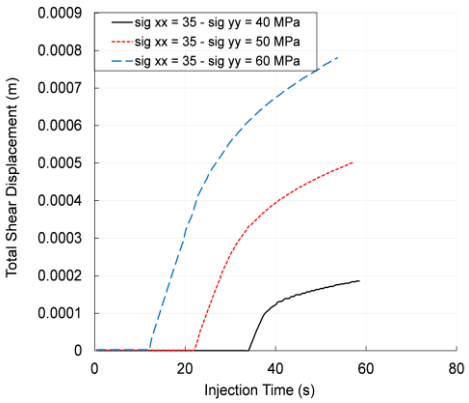

Figure 5. Shear displacement at injection point.

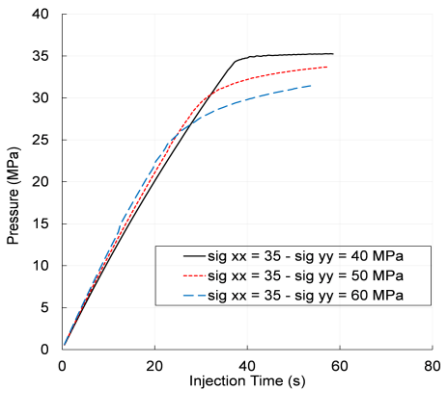

Figure 6. Pressure-Time profile at injection point.

The mechanism by which the stress state is changed in this study is through injection into the natural fracture and the applied far-field stresses are fixed. To date, the literature is mostly concerned with propagation of dry natural fractures under compression and wing crack propagation is triggered by increasing the maximum principal stress as a common practice. Consequently, the amount of shear stress provided by increasing the maximum principal stress is not limited. However, the maximum shear stress in this study is controlled by the initial state of stress.

3.3 Stress State, Constant Differential Stress

In this example a 45 degree crack is subject to different sets of in-situ stresses having an equal differential stress, $\sigma_{yy} - \sigma_{xx}$. The differential stress is 20 MPa in all the cases while the minimum and maximum compressive stresses vary from one case to another. The pressure-time plots for this example are shown in Figure 7. It is evident in Figure 7 that the pressure at the injection point is lower than the minimum compressive stress in all three cases. Although the differential stress is similar for these cases, the normal stress acting on

the natural fracture surfaces are different which results in different propagation behavior. The onset of propagation which is marked by the change of slope on the pressure-time plot is different for the examples considered in this section. Figure 9 shows the geometry of the pre-existing natural fractures and the propagated wing cracks. It can be observed in this figure that for a given injection time, the wing cracks are longer at lower in-situ stresses as compared to higher in-situ stresses. This is in fact due to the higher local compressive stresses at the crack tip in higher in-situ stress condition. Therefore, for a given differential stress, wing cracks are more likely to propagate at lower in-situ stress regions of a reservoir.

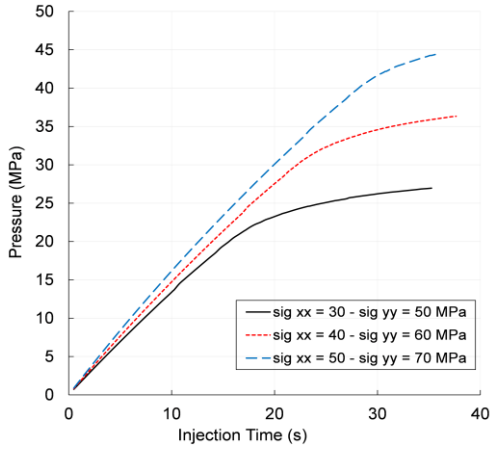

Figure 7. pressure-time profile at injection point.

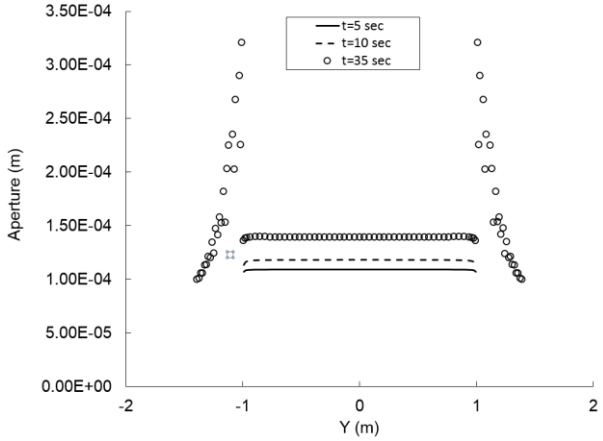

Figure 8. Natural fracture aperture profile at different injection times ($\sigma_{xx} = 30, \sigma_{yy} = 50$ MPa).

Natural fracture aperture history is another important parameter to explore in a natural fracture propagation problem. Figure 8 shows natural fracture aperture profile at different injection times for the case of $\sigma_{yy} = 50$ and $\sigma_{xx} = 30$ MPa. The hydraulic aperture profile along the natural fracture is plotted at different injection times before and after the propagation. The solid and the dashed line on Figure 8 show the natural fracture aperture before propagation. It can be observed in this figure that the aperture increases due to injection. It is interesting to notice that the elements on the wing crack have significantly higher apertures as compared to the elements along the pre-existing natural fracture. Moreover, the hydraulic aperture is higher at the bottom of wing cracks as compared to the tip of the wing cracks.

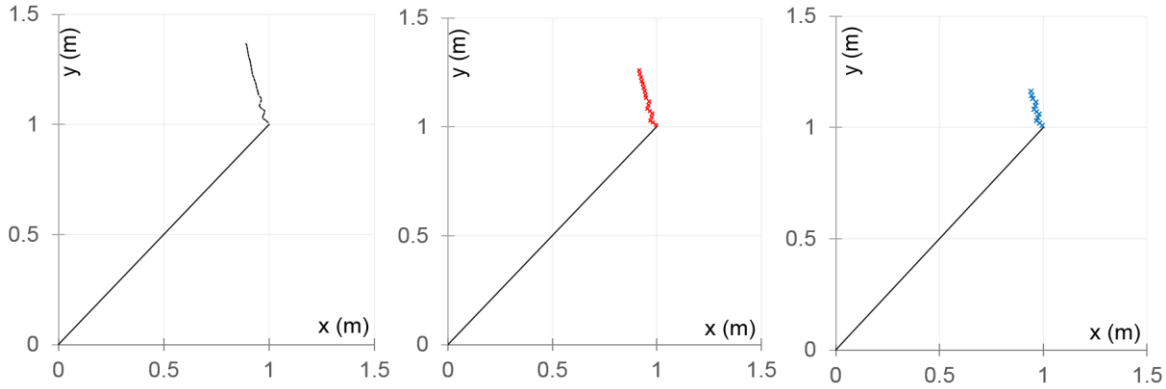

Figure 9. Upper half of the crack (a) $\sigma_{xx} = 30, \sigma_{yy} = 50$ MPa (b) $\sigma_{xx} = 40, \sigma_{yy} = 60$ MPa (c) $\sigma_{xx} = 50, \sigma_{yy} = 70$ MPa.

3.4 Intact Rock Cohesion

This example is designed to illustrate the importance of the shear strength of the intact rock and how it impacts the different modes of propagation of a closed natural fracture. In this example, a 45 degree crack is subject to 35 and 50 MPa of in-situ stresses and the cohesion of the intact rock ranges from 8 to 10 MPa. The other parameters used in this example are summarized in Table 1.

It is well known in the literature that the mode I propagation usually occurs before the Mode II propagation in brittle materials. However, the propagation of closed cracks in shear mode has also been observed in the experiments and numerical studies. Shear propagation begins once the local shear stress at the tip of the pre-existing natural fracture exceeds the local shear strength. The mode of propagation is expected to be greatly impacted by the cohesion of the intact rock. Figure 10 shows the pre-existing natural fracture and propagated segments for different values of intact rock cohesion. It can be observed in Figure 10 that both shear and wing cracks exist in Figure 10 (a) and the length of the shear crack (red dashed line) is almost equal to that of wing cracks. The length of the shear crack

decreases as the cohesion increases (see Figure 10 (b) and (c)). This is simply because of the higher shear strength at the crack tip that prevents shear propagation. It is interesting that shear crack propagates in a plane approximately parallel to the plane of the pre-existing natural fracture. The slight deviation from the original crack plane is believed to be due to the influence of the wing cracks on the local stresses at the kink point. The wing cracks and shear cracks may be less influenced by each other as they grow apart. This example shows that Mode I and Mode II propagation are both likely to occur in response to injection and the existence of shear cracks should not be neglected in reservoir stimulation. Furthermore, Mode II propagation in a closed natural fracture is closely related to the cohesion and the friction parameters of the intact rock and shear propagation becomes equally as important as wing cracks in the rocks with low shear strength. So that shear propagation is more likely in rocks that have many small crack and micro-cracks.

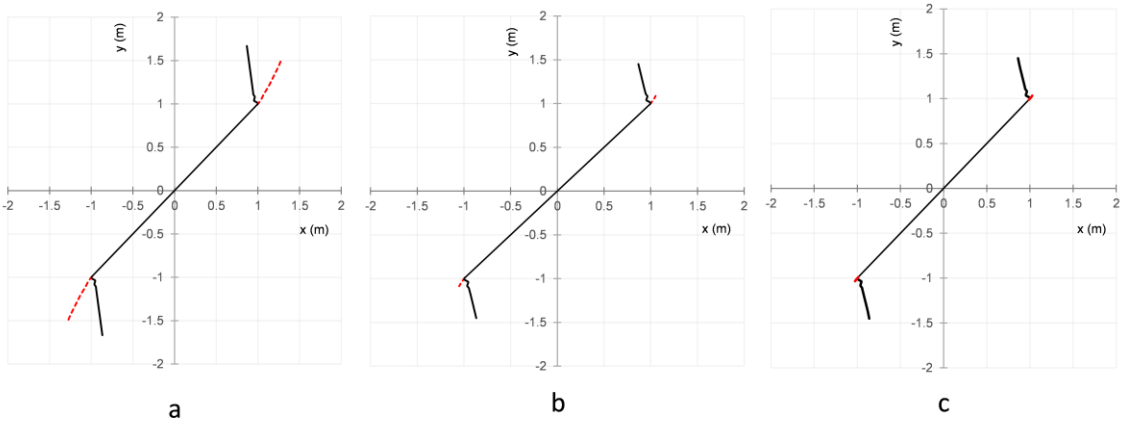

Figure 10. Wing crack and shear propagation for different rock cohesion values (a) $C' = 8$, (b) $C' = 10$, (c) $C' = 12$ MPa

The pressure profile for this example is shown in Figure 11. This figure shows that the pressure-time profile at the injection point almost coincides for c'=10 MPa and c'=12 MPa. This is in fact due to the same propagation behavior that is observed for these cases (see Figure 10 (b) and (c)). However, the pressure profile looks slightly different for the case of c'=8 MPa which is essentially because of the additional shear crack extension that was observed in this case.

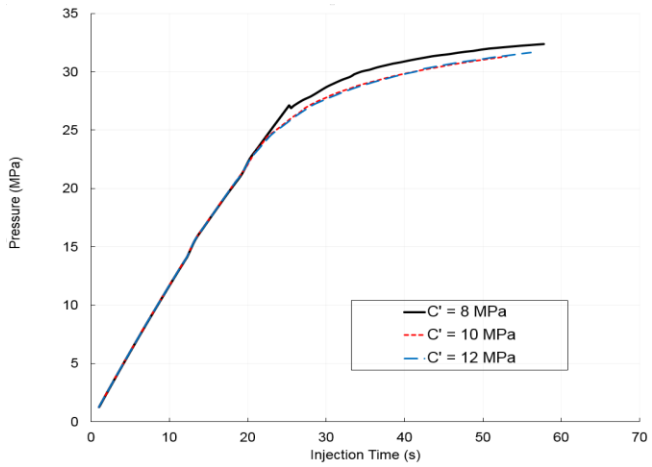

Figure 11. Pressure-Time profile at the injection point for three intact rock cohesion values

4. CONCLUSIONS

A displacement discontinuity model is developed to study the propagation of mechanically-closed natural fractures due to injection inside the natural fracture. Our results indicate that both Mode I and Mode II propagation are likely to occur and their relative dominance is a function of factors such as stress state, and rock and natural fracture properties (and likely temperature). Our simulations and analysis show that natural fracture stimulation may be accomplished by injection pressures below the minimum in-situ stress. The tendency for mode II propagation alongside the wing crack propagation was found to be higher at high dipping angles (60 degree) as compared to 30 and 45 degree natural fractures. The wing crack trajectory is found to be similar under constant confining stress while the pressure requirement for propagation is lower at higher initial differential stress values. Moreover, wing crack propagation is more likely at lower normal stresses (lower in-situ stresses for a given differential stress). Higher stress magnitudes tend to suppress the length of the wing cracks. The results show that the mode II propagation does occur and is greatly impacted by the intact rock cohesion. Both types of fracture growth occur in geothermal reservoir at pressures below the minimum in-situ stress, depending on the fracture morphology.

REFERENCES

Allodi, A., Castelli, M. and Scavia, C. 2002. Implementation Of The Slip-weakening Model in a Displacement Discontinuity Method Based Numerical Technique. *Boundary Elements XXIV*. WIT Press. WIT Transactions on Modelling and Simulation, Volume 32.

Bandis, S.C., Lumsden, A.C., and Barton, N.R. 1983. Fundamentals of Rock Joint Deformation. Int. J. Rock Mech. Min. Sci. & Geomech. Abstr. 20 (6): 249–268.

Bobet, A. and Einstein, H. H. 1998. Fracture coalescence in rock-type materials under uniaxial and biaxial compression. *Int. J. Rock Mech. Min. Sci*. 35(7): 863-889.

Bombolakis, E. G. 1973. Study of the Brittle Fracture Process under Uniaxial Compression. *Tectonophysics* 18 (3-4): 231-248

Brown, S.R., and Scholz, C.H. 1985. Closure of Random Elastic Surfaces in Contact. Journal of Geophysical Research 90 (B7): 5531-5545.

Cao, P., Liu, T. and Pu, C. et al. 2015. Crack propagation and coalescence of brittle rock-like specimens with pre-existing cracks in compression. *Engineering Geology*. 187: 133-121.

Cook, N.G.W. 1992. Natural Joints in Rock: Mechanical, Hydraulic, and Seismic Behavior and Properties under Normal Stress. *Int. J. Rock Mech. Min. Sci. & Geomech. Abstr*. 29 (3): 198–223.

Crouch, S.L. and Starfield, A.M. 1983. Boundary element methods in solid mechanics. 1st Ed. London: George Allen & Unwin.

Dobroskok, A., Ghassemi, A. and Linkov, A. 2005. Extended structural criterion for numerical simulation of crack propagation and coalescence under compressive loads. *Int. J. of Fracture*. 133 (3): 223-246.

Goodman, R.E. 1976. Methods of Geological Engineering in Discontinuous Rocks. 1st Ed. New York: West.

Hoek, E., Bieniawski, Z. T. 1984. Brittle fracture propagation in rock under compression. Int. J. Fracture 26: 276-294.

Horii, S., Nemat-Nasser, S. 1986. Brittle failure in compression: splitting, faulting and brittle-ductile transition. Phil. Trans. Roy. Soc. London, 319 (1549): 337-374.

Huang, K., Zhang, Z., Ghassemi, A. 2013. Modeling three-dimensional hydraulic fracture propagation using virtual multidimensional internal bonds. Int. J. Numer. Anal. Meth. Geomech. 37:2021–2038.

Jung, R. EGS — Goodbye or Back to the Future. 2013. Presented at International Conference for Effective and Sustainable Hydraulic Fracturing. Intech, Brisbane, Australia. 20-22 May 2013

Kamali, A. and Pournik, M. 2015. An Investigation of Rough Surface Closure with Application in Fracturing. Presented at American Rock Mechanics Association conference held in San Francisco, June 28th -July 1st

Li, Y., Chen, L. and Wang, Y. 2005. Experimental research on pre-cracked marble under compression. *International Journal of Solids and Structures*. 42 (9-10): 2505-2516.

Nemat-Nasser, S., and Horii, S. 1983. Rock failure in compression. Proceedings 9th Workshop Geothermal Reservoir Engineering Stanford University, Stanford, California.

Petit, J., Barquins, M. 1988. Can natural faults propagate under Mode II conditions?. *Tectonics*. 7 (6): 1243-1256

Rao, Q., Sun, Z., Stephansson, O. et al. 2003. Shear Fracture (Mode II) of Brittle Rock. *Int. J. Rock Mech. Min. Sci.* 40 (3): 355-375.

Ghassemi, A., Tarasovs, S., and Cheng, A. H.-D. 2007. A three-dimensional study of the effects of thermo-mechanical loads on fracture slip in enhanced geothermal reservoir. Int. J. Rock Mechanics & Min Sci., Vol. 44, pp. 1132–1148

Scavia, C. 1995. A Method for the Study of Crack Propagation in Rock Structures. *Geotehcnique* 45 (3): 447-463.

Shen, B. and Stephansson, O. 1994. Modification of the G-Criterion for Crack Propagation Under Subjected to Compression. *Engineering Fracture Mechanics*. 47 (2): 177-189.

Stone, T. J., Babuska, I. 1997. A numerical method with a posteriori error estimation for determining the path taken by a propagating crack. *Computer Methods in Applied Mechanics and Engineering*. 160 (3-4): 245-271.

Vesarhelyi, B. and Bobet, A. 2000. Modeling of Crack Initiation, Propagation and Coalescence in Uniaxial Compression. *Rock Mech. Rock Engng*. 33 (2): 119-139.